ADVANCED MATERIALS

Supporting Information

for *Adv. Mater.*, DOI: 10.1002/adma.201200540

Path-Guided Wrinkling of Nanoscale Metal Films

Chuan Fei Guo, Vishal Nayyar, Zhuwei Zhang, Yan Chen, Junjie Miao, Rui Huang, and Qian Liu**

Submitted to ADVANCED MATERIALS

Supplementary information

Title: Path-guided wrinkling of nanoscale metal films

By *Chuan Fei Guo, Vishal Nayyar, Zhuwei Zhang, Yan Chen, Junjie Miao, Rui Huang**, and *Qian Liu**

Prof. Qian Liu, Dr. Chuan Fei Guo, Dr. Zhuwei Zhang, Dr. Junjie Miao
Address: National Center for Nanoscience and Technology (China), No. 11 Beiyitiao, Zhongguancun Beijing 100190, China
E-mail: liuq@nanoctr.cn

Prof. Rui Huang, Mr. Vishal Nayyar
Address: Department of Aerospace Engineering and Engineering Mechanics, University of Texas, Austin TX 78712, USA
E-mail: ruihuang@mail.utexas.edu

Dr. Yan Chen
Institute of Mechanics, Chinese Academy of Sciences, No. 15 Beisihuanxi Road, Beijing 100190, China

Keywords: wrinkling, laser direct writing, surface patterns, thin films

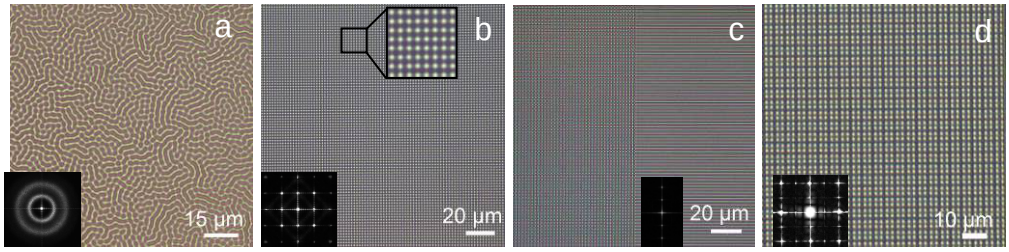

Figure S1. Large area fabrication of surface structures via wrinkling. **a**, Isotropic wrinkling without GPs. **b**-**d**, Highly ordered wrinkle patterns directed by GPs. Insets show the corresponding FFT patterns.

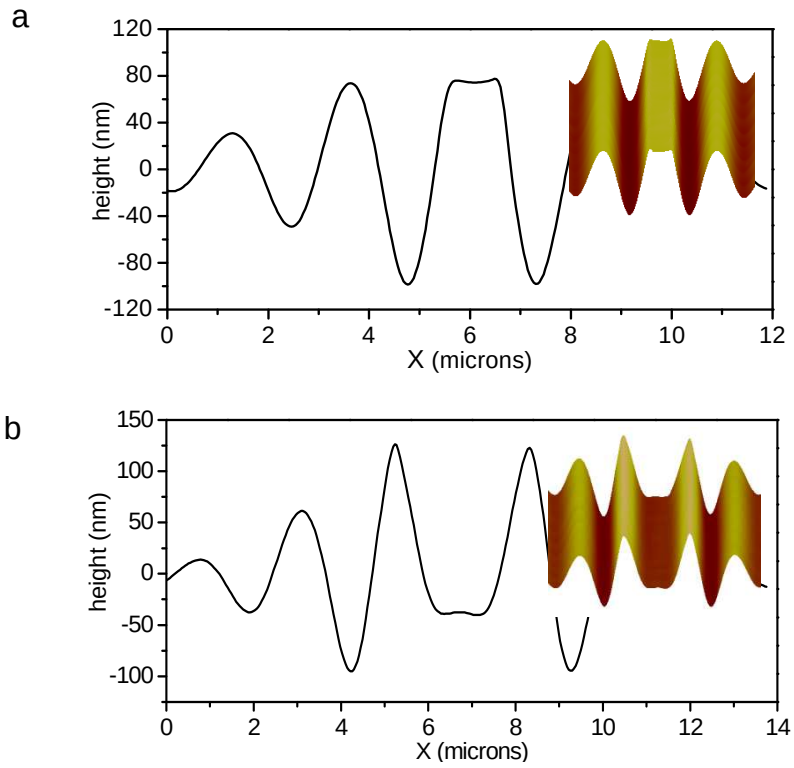

Figure S2. Path-guided wrinkling can generate diverse surface structures, not limited to sinusoidal profiles. **a** and **b** show trapezoidal and inverted-trapezoidal profiles, respectively.

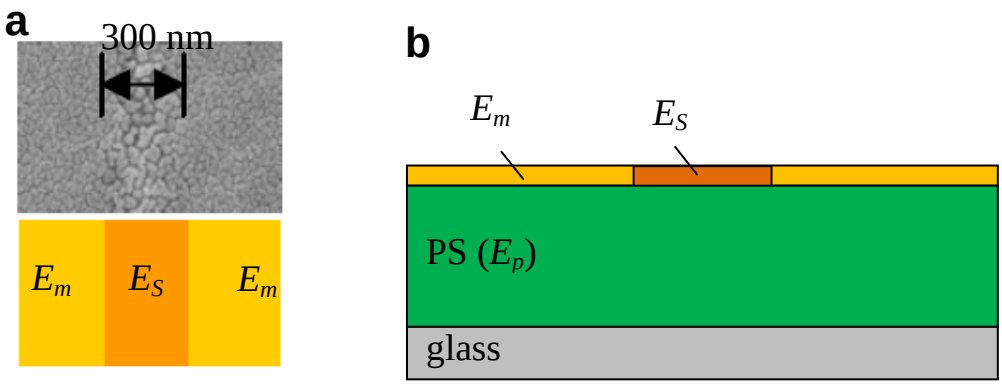

Figure S3. **a**, SEM image of the film surface shows morphological difference between laser exposed and unexposed areas. Apparently, the laser exposed area has a lower densification. **b**, A composite film model, in which the elastic modulus of the film is assumed to be lower in the laser exposed area ($E_S < E_m$).

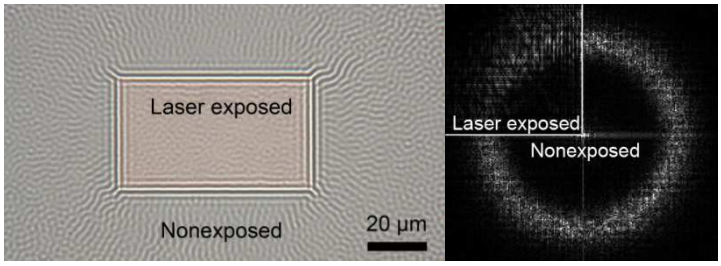

Figure S4. Wrinkling of a gold film with a large rectangular area exposed to laser. The corresponding FFT pattern shows that the wrinkle wavelength in the laser exposed area is smaller than in the unexposed area.

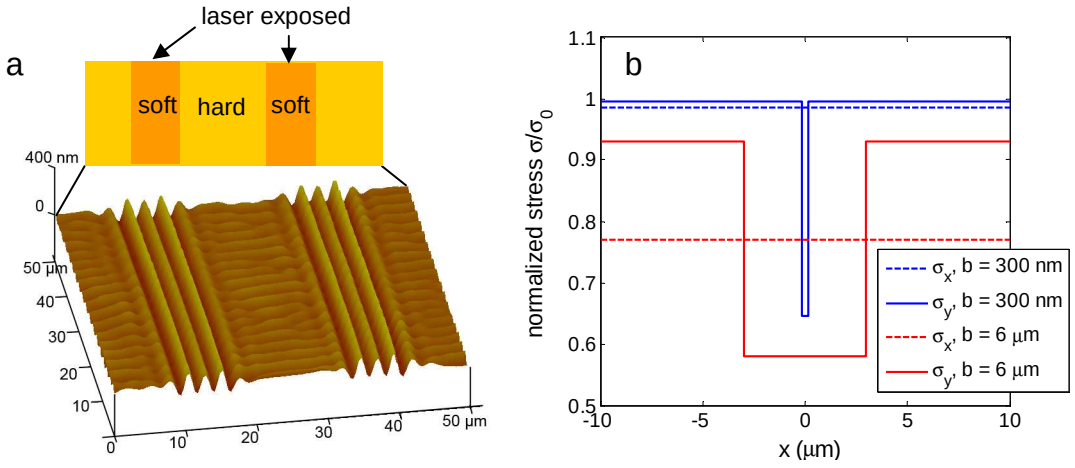

Figure S5. **a**, When the feature size of the laser exposed pattern is several times the intrinsic wrinkle wavelength, wrinkles are aligned parallel to the pattern boundaries in the exposed area but perpendicular to the boundaries in the unexposed areas, similar to the wrinkle patterns in Huck et al.[3] **b**, Finite element analysis of pre-wrinkling stress distributions in the metal film for a narrow and a wide GPs (GP width b = 300 nm and 6 μm, respectively). We assume that the Young's modulus in the GPs is 0.5 E_m, where E_m is the Young's modulus outside the GPs. The stresses are normalized by the reference stress for the case of a homogeneous film ($\sigma_x = \sigma_y = \sigma_0$). Since the PS underlayer is very soft at the elevated temperature ($T > T_g$), the stress along the x direction (σ_x) is nearly uniform in the film, while the stress in the y direction (σ_y) is much lower inside the GPs. For the narrow GP (b = 300 nm), σ_x is very close to σ_y outside the GP. For the wide GP (b = 6 μm), σ_x is much lower than σ_y outside the GP. The relative magnitudes of the two stresses are consistent with the observed wrinkle alignments inside and outside the GPs in **a**.

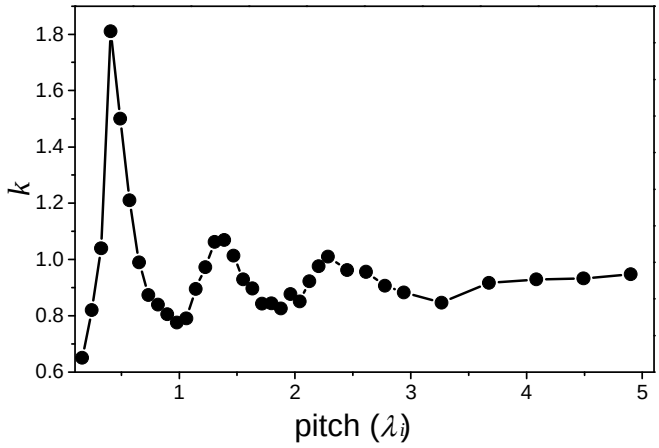

Figure S6. The dimensionless parameter *k* was determined as a function of the pitch (*d*) by comparing experimental data of two parallel unit-wrinkles with the superposition prediction in Eq. (2). For relatively large pitches ($d > 4\ \lambda_i$), *k* is approximately 1, suggesting a linear superposition. For relatively small pitches, however, *k* varies with *d* and oscillates around 1, possibly due to nonlinear effect of the interaction.

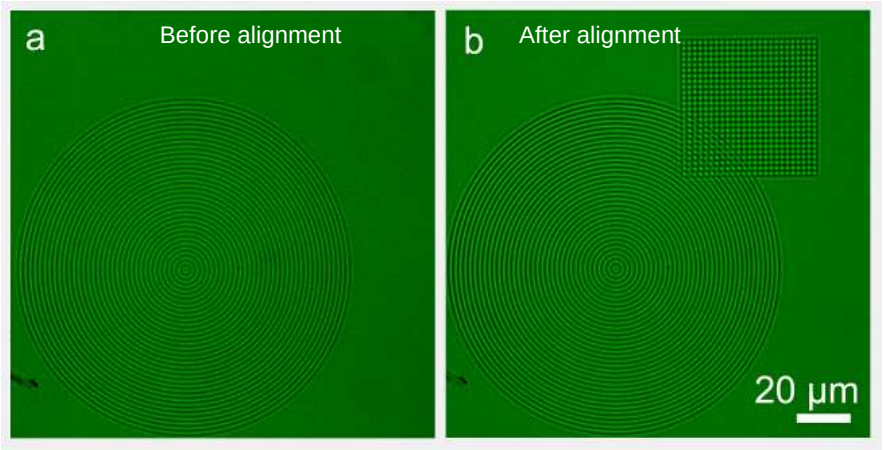

Figure S7. Alignment of wrinkle patterns: new wrinkle patterns can be generated by rewriting and heating. It provides the possibility to alter wrinkle structures. Note that the unexposed area is featureless.

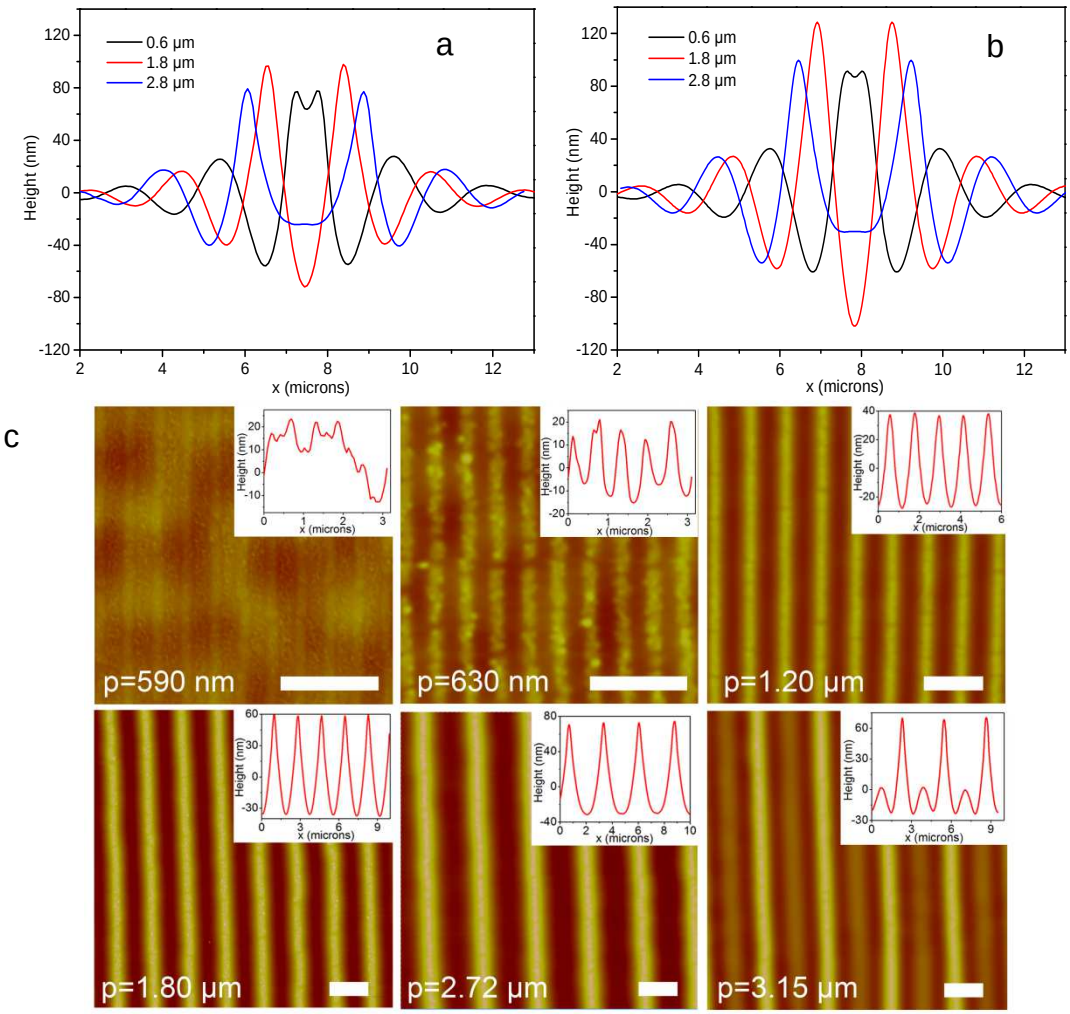

Figure S8. Pitch control of wrinkles. **a**, Experimental surface profiles of wrinkle patterns with two parallel GPs that have pitches of 0.6, 1.8 and 2.8 μm, respectively. **b**, Calculated surface profiles by superposition of two unit-wrinkles with pitches of 0.6, 1.8 and 2.8 μm, in good agreement with the experimental results in a. **c**, AFM images of parallel wrinkles formed by using multiple GPs with pitches (p) of 590 nm, 630 nm, 1.20 μm, 1.80 μm, 2.72 μm and 3.15 μm. Scale bars are 2 μm. Insets are corresponding profiles by crosssectional analysis.

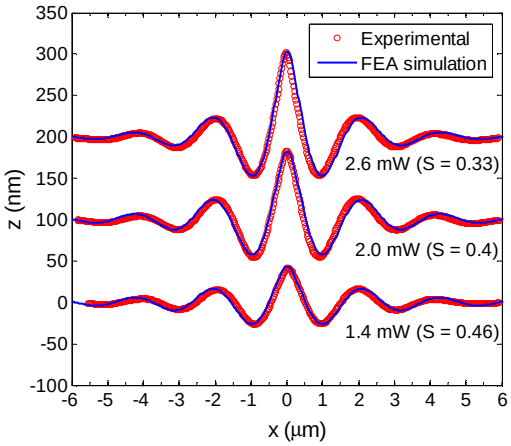

Figure S9. Profiles of unit wrinkles obtained with different laser powers, in comparison with finite element simulations of the composite film wrinkling with different softening parameters. The 0th order wrinkle amplitude increases with decreasing Young's modulus in the softer region, due to increasing laser power.

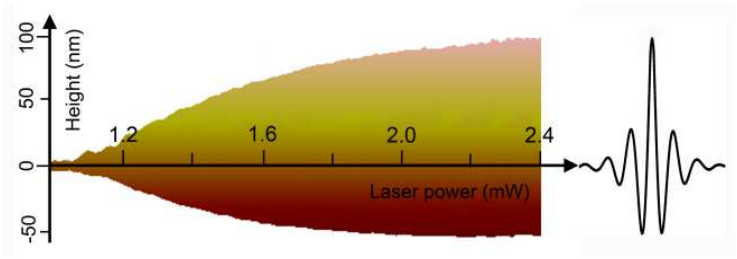

Figure S10. Variation of the wrinkle height with the laser power along one straight GP, corresponding to the wrinkle pattern shown in Figure 3b.

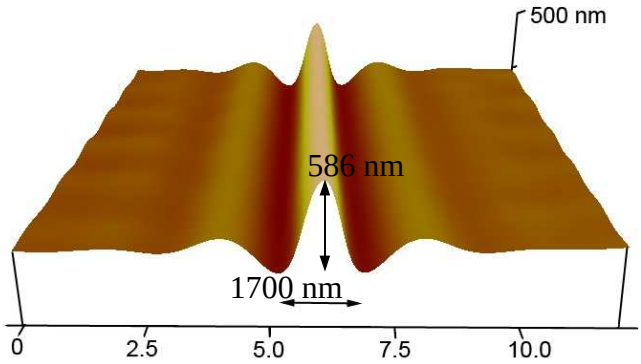

Figure S11. A unit-wrinkle with an aspect ratio of 0.34. The height is 586 nm and the width is 1700 nm. Such unit-wrinkles can be obtained by heating the bilayer at 140℃ for several hours.

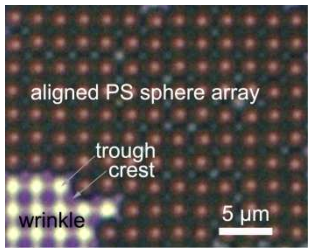

Figure S12. Tetragonal egg-crate structure for aligning PS microspheres, clearly demonstrating that all microspheres are located on the troughs and form a tetragonal lattice. On a smooth surface, the microspheres tend to form a hexagonal lattice, which is a stable structure. The tetragonal lattice is a metastable structure that can hardly be assembled on smooth surfaces.

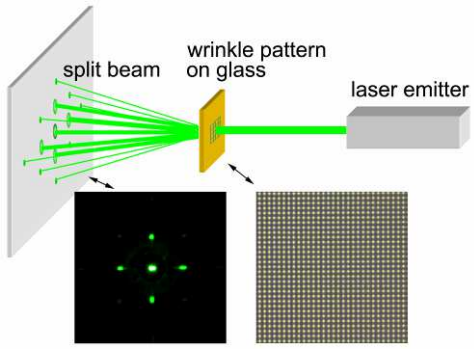

Figure S13. Schematic illustration of a two-dimensional wrinkle pattern used as beam splitter, showing the optical image of the surface wrinkle pattern and the corresponding diffraction pattern.

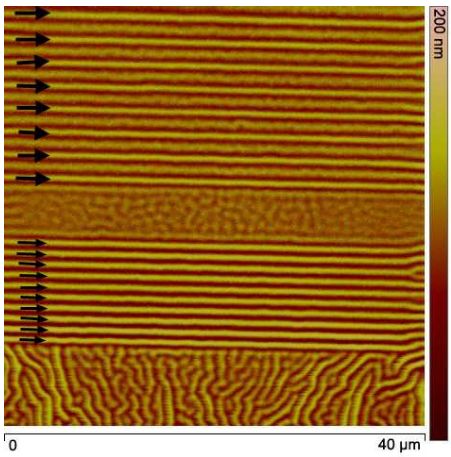

Figure S14. Path-guided wrinkling of a Sn/PS bilayer (40 μm × 40 μm). The black arrows indicate guiding paths.

Appendix

Section A. Intrinsic wrinkle wavelength

For the Au/PS bilayer system, the intrinsic wrinkle wavelength depends on the thickness and elastic modulus of both layers. An approximate formula to predict the intrinsic wavelength is:[1,2]

$$\lambda_i = 2\pi h_m \left[\frac{(1+\nu_p)(1-2\nu_p)}{12(1-\nu_p)(1-\nu_m^2)} \frac{E_m h_p}{E_p h_m} \right]^{1/4}, \quad \text{(S1)}$$

where h, E and ν are the thickness, Young's modulus and Poisson ratio, with the subscripts m and p for the metal and polymer layers, respectively. Experimentally the intrinsic wrinkle wavelength can be determined from the isotropic wrinkle pattern as shown in Figure S1a. Taking h_m = 6 nm, h_p = 300 nm, E_m = 78 GPa, E_p = 26 kPa, ν_m = 0.3 and ν_p = 0.35, we obtain λ_i = 2.04 μm, in good agreement with the experiment. Note that Eq. (S1) is valid only for the bilayer system with $\nu_p < 0.5$ and $h_p < \lambda_i$.[1,2]

Section B. Surface profile of a unit-wrinkle

The profile of a unit-wrinkle as shown in Figure 2a can be described approximately by Eq. (2). Since the width of GP (~300 nm) is much smaller than the intrinsic wrinkle wavelength (~2.1 μm), the peak-to-peak distance of the unit-wrinkle is approximately equal to the intrinsic wavelength. On the other hand, the wrinkle height at the center of GP (A_0) and the damping length (l_c) depend on the laser power as well as the modulus ratio and the thickness of the bilayer. Both A_0 and l_c can be determined experimentally by comparing the measured unit wrinkle profile to Eq. (2). In Figure 2a, A_0 = 108 nm and $l_c = 0.7\ \lambda_i$ were used to fit the experimental data.

The unit-wrinkle profile can be predicted by numerical simulations based on the composite film model (Figure S3). A two-dimensional finite element model was constructed using the commercial package ABAQUS (version 6.9, SIMULIA). Both the metal film and

PS layer are assumed to be linear elastic. To match the intrinsic wrinkle wavelength, we take h_m = 6 nm, h_p = 300 nm, E_m = 78 GPa, E_p = 26 kPa, ν_m = 0.3 and ν_p = 0.35. In the laser exposed area, the Young's modulus of the metal film is assumed to be lower, $E_S = S\,E_m$, where S is the softening parameter ($0 < S < 1$). The width of the GP is b (= 300 nm) and the length of the bilayer model is L (= 14 μm). The bilayer is subject to plane-strain compressive displacement at both ends whereas the bottom surface remains flat and the top surface is traction free. First, an eigenvalue analysis is performed to predict the critical strain for the onset of wrinkling and the mode shape. Subsequently, the profile of the unit wrinkle is simulated for increasing strain (ε) by a post-buckling analysis. To compare with the experimental data, we vary S and ε. As shown in Figure 2a, by using S = 0.4 and ε = –0.334%, the predicted wrinkle profile agrees closely with the experimental data.

Section C. Effect of laser exposure

Based on the SEM image in Figure S3, it is assumed that the Young's modulus of the metal film is lowered in the laser exposed area. To estimate the Young's modulus in the laser exposed area, an experiment was conducted with a large rectangular area of the gold film exposed to laser. Wrinkles were observed in both laser exposed and unexposed areas (Figure S4), and the wrinkle wavelengths were measured. It is found that the wrinkle wavelength is shorter in the laser exposed area, further supporting the hypothesis that laser exposure lowers the Young's modulus of the metal film. Quantitatively, the wrinkle wavelength in the laser exposed area collected from several samples is approximately 0.8-0.9 λ_i, where λ_i is the wrinkle wavelength in the un-exposed area. By Eq. (S1), the Young's modulus of the film in the laser exposed area is estimated to be 0.40-0.66 E_m, corresponding to a softening parameter S = 0.4-0.66. We note that the laser exposure may also change other properties of the film, such as Poisson's ratio and the coefficient of thermal expansion, which are not considered in the present analysis.

References

[1] Huang, R. Kinetic wrinkling of an elastic film on a viscoelastic substrate. *J. Mech. Phys. Solids* **53**, 63–89 (2005).

[2] Huang, Z. Y., Hong, W., Suo, Z. Nonlinear analyses of wrinkles in a film bonded to a compliant substrate. *J. Mech. Phys. Solids* 53, 2101–2118 (2005).

[3] Huck, W. T. S. *et al*. Ordering of spontaneously formed buckles on planar surfaces. *Langmuir* **16**, 3497–3501 (2000).